

Coupled frustrated quantum spin-1/2 chains with orbital order in volborthite $\text{Cu}_3\text{V}_2\text{O}_7(\text{OH})_2 \cdot 2\text{H}_2\text{O}$

O. Janson,^{1,*} J. Richter,² P. Sindzingre,³ and H. Rosner^{1,†}

¹*Max-Planck-Institut für Chemische Physik fester Stoffe, D-01187 Dresden, Germany*

²*Institut für Theoretische Physik, Universität Magdeburg, D-39016 Magdeburg, Germany*

³*Laboratoire de Physique Théorique de la Matière Condensée, Univ. P. & M. Curie, Paris, France*
(Dated: November 20, 2018)

We present a microscopic magnetic model for the spin-liquid candidate volborthite $\text{Cu}_3\text{V}_2\text{O}_7(\text{OH})_2 \cdot 2\text{H}_2\text{O}$. The essentials of this DFT-based model are (i) the orbital ordering of Cu(1) $3d_{3z^2-r^2}$ and Cu(2) $3d_{x^2-y^2}$ (ii) three relevant couplings J_{ic} , J_1 and J_2 (iii) the ferromagnetic nature of J_1 and (iv) frustration governed by the next-nearest-neighbor exchange interaction J_2 . Our model implies magnetism of frustrated coupled chains in contrast to the previously proposed anisotropic kagome model. Exact diagonalization studies reveal agreement with experiments.

PACS numbers: 71.20.Ps, 75.10.Jm, 75.25.Dk, 91.60.Pn

I. INTRODUCTION

The search for new magnetic ground states (GS) is a major subject in solid state physics. Magnetic monopoles in the spin ice system $\text{Dy}_2\text{Ti}_2\text{O}_7$ (Ref. 1–3), the metal-insulator transition in the spin-Peierls compound TiOCl 4 and the quantum critical behavior in $\text{Li}_2\text{ZrCuO}_4$ 5,6 are among recent discoveries that demonstrate the power of combining precise experimental techniques with modern theory. However, for a rather large number of problems experiment and theory don't keep abreast, since it is often tricky to find a real material realization for a well studied theoretical model. The most remarkable example is the concept of a “resonating valence bond”⁷ — a magnetic GS formed by pairs of coupled spin-singlets lacking the long range magnetic order (LRO). Subsequent studies revealed a fascinating variety of disordered GS,^{8,9} commonly called “spin liquids” in order to emphasize their dynamic nature, and even raised the discussion of their possible applications.¹⁰

Following the common belief that the spin liquid GS may emerge from the interplay of low-dimensionality, quantum fluctuations and magnetic frustration, considerable effort has been spent on the search for spin-1/2 Heisenberg magnets with kagome geometry. The synthesis of herbertsmithite $\text{Cu}_3\text{Zn}(\text{OH})_6\text{Cl}_2$ 11, the first inorganic spin-1/2 system with ideal kagome geometry, and subsequent studies revealed besides the desired absence of magnetic LRO¹² (i) intrinsic Cu/Zn structural disorder and (ii) the presence of anisotropic interactions complicating the spin physics.¹³ The recently synthesized kapellasite¹⁴ was predicted to imply modified kagome physics due to an additional relevant coupling.¹⁵

Since the search for a system representing the pure kagome model is far from being completed, it is natural to consider systems with lower symmetry where the distortion is small enough to keep the essential physics.¹⁶ This way, the attention has been drawn to the mineral volborthite $\text{Cu}_3\text{V}_2\text{O}_7(\text{OH})_2 \cdot 2\text{H}_2\text{O}$, where the Cu sites form a slightly distorted kagome network.¹⁷ However, the local

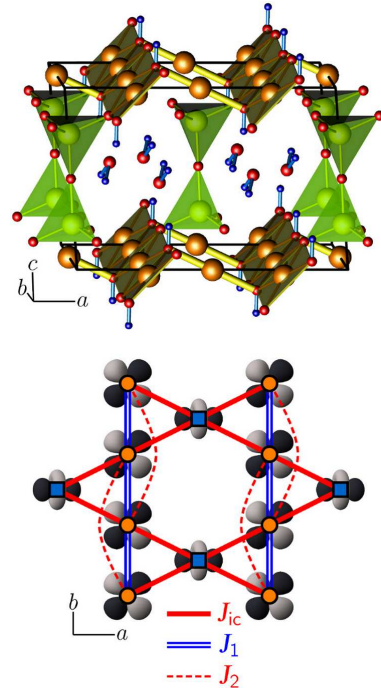


FIG. 1: (Color online) Top: $\text{Cu}(1)\text{O}_2$ dumbbells (yellow), $\text{Cu}(2)\text{O}_4$ plaquettes (dark yellow), V_2O_7 pyrovanadate groups (connected green tetrahedra) and H_2O molecules in volborthite. Only short Cu–O bonds are shown. Bottom: a distorted kagome layer in the crystal structure of volborthite. The magnetically active orbitals and leading exchange couplings are shown.

environment of two independent Cu sites is essentially different: Cu(1) forms dumbbells of two short Cu–O bonds (and four long Cu–O bonds; “2+4”), while Cu(2) resides in a plaquette formed by four short bonds (Fig. 1, top). Recently, DFT studies of CuSb_2O_6 , implying the “2+4” local environment of Cu atoms, revealed that orbital ordering (OO) drastically changes the nature of the magnetic coupling from three-dimensional (3D) to one-dimensional (1D).¹⁸ The crucial impact of OO onto mag-

netism of volborthite will be in the focus of this paper.

The availability of a pure powder and negligible structural disorder in volborthite inspired thorough experimental studies of its magnetic properties. The magnetic GS was recently investigated by ^{51}V nuclear magnetic resonance (NMR),¹⁹ following earlier NMR,²⁰ high-field electron spin resonance²¹ and muon spin relaxation²² studies. The GS is characterized by the absence of magnetic LRO, high density of low energy excitations and two distinct scales of spin fluctuations. At 4.5 Tesla, volborthite undergoes a transition to another magnetic phase. The fingerprint of this transition is a step-like feature in the magnetization curve. Similar features are observed at 25 and 46 Tesla, hinting at a series of successive transitions.²³ Between 60 and 70 Tesla, the slope of magnetization diminishes indicating a possible onset of a magnetization plateau.²⁴ Magnetic susceptibility measurements yield a broad maximum at temperatures much smaller than the Curie-Weiss temperature, indicating strong frustration.

Extensive experimental information stimulated theoretical studies aiming to find a consistent description for magnetism of volborthite. Since the pure kagome model doesn't account for the experimental data, the studies were focused on the GS and thermodynamical properties of the anisotropic kagome model (AKM). However, attempts to reach consistency by varying the degree of anisotropy were not satisfying so far. The most striking disagreement is the deviation of the theoretical magnetic susceptibility χ even at rather high temperatures ($T \sim J$).²⁵

This disagreement originates from the choice of the AKM which was based on geometry only, while the structural peculiarities of volborthite were not considered. A standard tool to treat such peculiarities properly is density functional theory (DFT) calculations that can provide a reliable microscopically based model.^{4,5,15,26,27} Here, we show that DFT calculations yield an unexpected microscopic magnetic model for volborthite, moving away from the kagome model. Moreover, we reveal strong similarities to the physics of frustrated coupled chains due to OO. Our subsequent simulations of the microscopic model evidence an improved agreement with the experimental data.

II. DFT CALCULATIONS

The DFT calculations have been performed in the local density approximation (LDA) using the full potential²⁸ code `fplo8.65-32`.²⁹ For the scalar relativistic calculations, the Perdew and Wang parametrization³⁰ of the exchange-correlation potential has been used. All calculations have been performed on well-converged k -meshes.³¹

The reliability of DFT calculations depends crucially on the accuracy of the experimental structural data used as input. The chemical composition of volborthite ham-

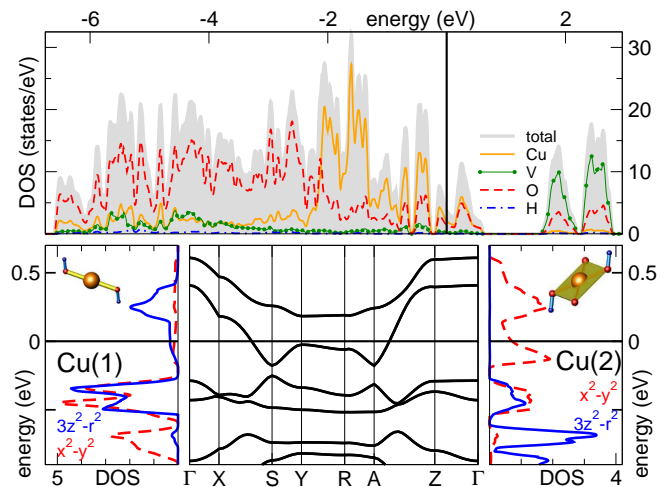


FIG. 2: (Color online) Density of states (upper panel), the band structure (lower panel, center) and the orbital-resolved density of states for Cu(1) (left) and Cu(2) (right) of the optimized structure ($3d_{x^2-y^2}$ is shown with a dashed line).

pers structural studies due to the considerable content of V and H atoms, which are poor scatterers of neutrons and x-rays, respectively. Therefore, prior to investigations of subtle electronic effects, the structural data should be addressed. Among several structural data sets available we have chosen a structural model (exp) based on joint x-ray and neutron diffraction studies. Although such combination improves the reliability of the resulting data, the statistics (number of reflections) is not sufficient for fully conclusive results. Therefore, we have carried out a structural optimization relaxing the atomic coordinates and minimizing the forces, since LDA calculations for cuprates usually yield accurate and consistent results.^{15,16,32} Moreover, to evaluate the influence of the different structural models, we perform calculations for the experimental as well as for the optimized structure.

The LDA-optimized crystal structure (opt) yields considerably lower total energy and atomic forces. Although individual bond lengths and angles change up to several percents (O-H distance increased by $\sim 10\%$), the overall structural motive and the different local environment of Cu(1) and Cu(2) are inherited from the original model.

LDA yields a valence band width of 7 eV (Fig. 2) typical for cuprates, and a metallic GS in contrast to the green, transparent samples. This well-known problem of the LDA originates from the underestimation of strong on-site correlations for a Cu $3d^9$ configuration. Nevertheless, LDA is a reliable tool to evaluate the relevant orbitals and couplings.³¹ For most cuprates, an effective one-band model is well justified by a band complex at Fermi level (ϵ_F) formed by N antibonding bands, where N is the number of Cu atoms per cell. In contrast, in volborthite ($N = 3$), six bands in vicinity of ϵ_F (Fig. 2) evidence a sizable hybridization of two different $3d$ orbitals at each Cu site that need to be included into the modeling.

The relevant Cu $3d$ orbitals are revealed by projecting the density of states (DOS) onto local orbitals. The resulting orbital-resolved DOS is shown in Fig. 2. For both Cu(1) and Cu(2), the $3d_{x^2-y^2}$ and $3d_{3z^2-r^2}$ states are relevant and hybridized with each other. To evaluate the relevant couplings, we consider two orbitals ($3d_{x^2-y^2}$ and $3d_{3z^2-r^2}$) per Cu atom and fit the six bands using the Wannier functions (WFs) technique.^{31,33}

Prior to evaluation of the relevant couplings, the correct orbital GS should be found. LDA yields an essentially different filling of the orbitals: for Cu(1) the $3d_{3z^2-r^2}$ is close to half-filling and the $3d_{x^2-y^2}$ is almost filled (Fig. 2, left), while for Cu(2) it is the other way round (Fig. 2, right). However, the closer proximity to half-filling in the LDA picture does not necessarily provide the correct answer, as revealed for the related system CuSb₂O₆.¹⁸ Thus, we cross-check the LDA result by LSDA+ U calculations. In agreement with the LDA, the latter yield the magnetically active Cu(1) $3d_{3z^2-r^2}$ and Cu(2) $3d_{x^2-y^2}$ (see details below).

The relevant transfer integrals can be extracted from the WFs considering the hoppings between the GS orbitals (Cu(1) $3d_{3z^2-r^2}$ and Cu(2) $3d_{x^2-y^2}$). The leading terms are t_1 and t_{ic} , which coincide with two NN couplings in the AKM (Fig. 1, bottom). Surprisingly, the next-nearest-neighbor (NNN) coupling t_2 is also sizable, while other couplings are considerably smaller. A small value of the inter-layer coupling supports the 2D nature of magnetism.

The correct description of the orbital GS requires an appropriate description of correlations in the Cu $3d$ shell, which can be treated in a mean-field way using the LSDA+ U scheme. By stabilizing solutions comprising different orbital occupations and a subsequent comparison of their total energies, we evaluate the orbital GS. The separation between the orbital GS and the lowest lying excited orbital state ($3d_{x^2-y^2}$ for Cu(1) and Cu(2)) exceeds 500 meV (~ 6000 K), almost two orders of magnitude larger than the magnetic exchange (~ 100 K). Therefore, orbital and spin degrees of freedom are mostly decoupled and can be analyzed separately.

The leading exchange integrals J_1 , J_2 and J_{ic} are obtained mapping the results of LSDA+ U total energy calculations onto a Heisenberg model.³⁴ A careful analysis of the results shows that the individual values of exchange integrals are sensitive to (i) the structural model, (ii) the Coulomb repulsion U_d and (iii) the double-counting correction (DCC) scheme.³⁵ The crucial influence of these parameters is visualized in Fig. 3, where the results for the experimental and optimized structures are shown. For each structural model, we use the limiting cases for the DCC — around-the-mean-field (AMF) and the fully localized limit (FLL)³⁶ and vary U_d within a reasonable range.³⁷ Depending on these parameters, we obtain $J_1 = -80 \pm 10$ K, $J_2 = 35 \pm 15$ K and $J_{ic} = 100 \pm 60$ K for the experimental and $J_1 = -65 \pm 15$ K, $J_2 = 45 \pm 15$ K and $J_{ic} = 100 \pm 60$ K for the optimized lattice.

The substantially ferromagnetic nature of J_1 , in ac-

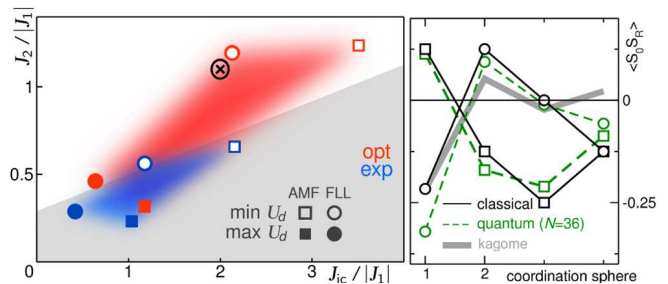


FIG. 3: (Color online) Left: exchange integrals as a function of the structural model (opt or exp), the LSDA+ U DCC scheme (AMF or FLL) and U_d (min U_d , max U_d) on the phase diagram of the J_1 - J_2 - J_{ic} model. The white and gray fields correspond to the singlet and the ferrimagnetic phases, respectively. The shaded areas depict possible values of exchange couplings for the both structural models. Our ED results yield the best agreement for $J_{ic}/|J_1| = 2$, $J_2/|J_1| = 1.1$, depicted by a cross. Right: correlation functions along (squares) and between (circles) the J_1 - J_2 chains deviate significantly from the kagome model (bold gray line).

cord with Goodenough-Kanamori-Anderson rules, and the relatively small uncertainties of its strength disregarding the parameters used give strong evidence that the pure kagome model is inappropriate for volborthite. The AKM can be ruled out since J_1 and J_{ic} support each other and do not give rise to frustration. Our microscopic insight evidences that an essentially different model with frustration governed by NNN exchange J_2 (competing with both J_1 and J_{ic}) should be used for volborthite. Despite sizable scattering of the J values, important general trends can be established. First, the optimized structure has an enhanced $J_2/|J_1|$ ratio compared to the experimental structure. Second, FLL yields considerably smaller J_{ic} and somewhat larger values for J_2 than AMF.

Based on DFT calculations, we obtain a microscopic magnetic model and determine the parameters J_1 , J_2 and J_{ic} . Although we find the relevant region in the phase space, the complexity of volborthite impedes a more accurate estimate of individual exchange integrals, especially J_{ic} . In this case, refining the parameters by numerical simulations of measured physical properties and subsequent comparison to experimental data is an appropriate way towards a deeper understanding.

III. EXACT DIAGONALIZATION

To realize a guided search for a consistent set of exchange integrals, the GS of the J_1 - J_2 - J_{ic} model should be investigated. We explore the phase space by considering a Heisenberg model with $J_1 < 0$, $J_2 > 0$, $J_{ic} > 0$. On a classical level, we find two GS: a ferrimagnetic (fM) phase with magnetization $m = 1/3$ and an incommensurate $m = 0$ helical (H) phase with spiral correlations along J_1 - J_2 frustrated chains, similar to those of edge

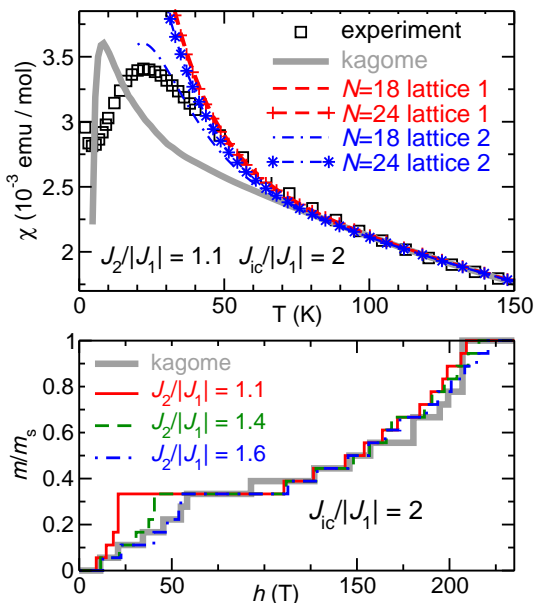


FIG. 4: (Color online) Top: fits to the experimental $\chi(T)$.²⁴ The solution of the J_1 - J_2 - J_{ic} model yields an improved description down to 50 K compared to the kagome model (bold gray line). Bottom: magnetization curves ($N=36$ sites) for different solutions of the J_1 - J_2 - J_{ic} model in comparison to the kagome model.

shared quasi 1D cuprates (see e.g. Ref. 5). The transition from the fM-phase to the H-phase is driven by the frustrating NNN in-chain coupling J_2 and occurs at $J_2^{class} = |J_1|/4 + J_{ic}/8$. To discuss the GS of the quantum model we use Lanczos exact diagonalization of finite lattices up to $N = 36$ sites.^{38,39} For the quantum model, the fM state competes with a singlet GS with $m = 0$, and the transition is given by $J_2^{quant} = 0.304|J_1| + 0.200J_{ic}$.⁴⁰ The transition line together with the DFT-derived exchange integrals are plotted in Fig. 3 (left). Since the experiments evidence zero magnetization of the GS, the fM solutions can be ruled out and the analysis can be restricted to the singlet GS.

To understand the nature of the GS, we consider spin correlations as a sensitive probe for magnetic ordering. While the correlations between the chains are similar to the standard kagome Heisenberg antiferromagnet, they are completely different along the J_1 - J_2 frustrated chains (Fig. 3, right). These in-chain correlations fit to a spiral state with a pitch angle very close to the classical model. Hence, our data suggest well pronounced in-chain spiral correlations together with weaker inter-chain correlations. We mention, however, that these statements are restricted to short-range correlations.

Since the magnetic correlations along the chains are strongest, one could argue that the model exhibits an effectively 1D low-temperature physics as has been discussed previously for other 2D models such as the crossed-chain model,⁴¹ anisotropic triangular lattice,⁴² as well as for modified kagome compounds.¹⁵ However, this

issue as well as a conclusive answer to the question of helical LRO need further investigation.

To comprise the experimental magnetization curve, we add the magnetic field term to the Heisenberg Hamiltonian and simulate the $m(h)$ dependence. For the boundary of the fM and singlet GS, we find a wide 1/3 magnetization plateau starting at $h_{c1} = 0$. However, the modification of the exchange parameters, in particular increasing of J_2 and decreasing of $|J_1|$ and J_{ic} , according to the limits set by DFT calculations leads to a significant increase of h_{c1} and to a drastic diminishing of the plateau width. Close to the DFT-boundary ($J_{ic}/|J_1| = 2$, $J_2/|J_1| = 1.1$, $J_{ic} = 100$ K), we obtain $h_{c1} = 22$ T, which is still smaller than the experimentally observed value. We should note that this deviation originates from the minimalistic character of the model and considerable finite size effects. Nevertheless, a slightly modified ratio $J_2/|J_1| = 1.6$ yields $h_{c1} = 55$ T (Fig. 4, bottom) in excellent agreement with the experiment. It should be mentioned that the nature of spin correlations in the 1/3-plateau phase is substantially different compared to the kagome model.⁴³ Small magnetization jumps seen experimentally²³ can not be resolved with present lattice sizes and might be related to anisotropic exchange.

We also calculate the temperature dependence of magnetic susceptibility $\chi(T)$ using two different lattices³¹ up to $N = 24$ sites. We obtain a good fit down to 50 K (Fig. 4, top),⁴⁴ the resulting $g = 2.16$ and $J_{ic} = 100.5$ K are in excellent agreement with experiments²¹ and our estimates from DFT.

IV. SUMMARY

To summarize, we suggest a new magnetic model for volborthite: assuming that DFT calculations are applicable to volborthite as they are for a plethora of compounds, the kagome model can be safely ruled out. Instead, the magnetism of volborthite is accounted for by a J_1 - J_2 - J_{ic} model reminiscent of coupled frustrated chains. For the proposed model, the orbital order of Cu(1) $3d_{3z^2-r^2}$ and Cu(2) $3d_{x^2-y^2}$ orbitals is crucial.

We suggest new experiments to challenge our model: resonant x-ray scattering measurements to study orbital effects and measurements in high magnetic fields (>70 Tesla) to get an access to the magnetization plateau. Additional investigations of the J_1 - J_2 - J_{ic} model itself by alternative simulation methods are desirable to clarify the influence of finite size effects, intrinsic for exact diagonalization.

ACKNOWLEDGEMENTS

We thank Z. Hiroi for providing us with $\chi(T)$ data. We acknowledge fruitful discussions and valuable comments from Z. Hiroi, F. Mila, G. Nilsen and A. Tsirlin.

- * Electronic address: janson@cpfs.mpg.de
† Electronic address: rosner@cpfs.mpg.de
- ¹ C. Castelnovo, R. Moessner, and S. L. Sondhi, *Nature* **451**, 42 (2008), arXiv:0710.5515.
 - ² L. D. C. Jaubert and P. C. W. Holdsworth, *Nature Phys.* **5**, 258 (2009), arXiv:0903.1074.
 - ³ D. J. P. Morris, D. A. Tennant, S. A. Grigera, B. Klemke, C. Castelnovo, R. Moessner, C. Czternasty, M. Meissner, K. C. Rule, J.-U. Hoffmann, K. Kiefer, S. Gerischer, D. Slobinsky, and R. S. Perry, *Science* **326**, 411 (2009).
 - ⁴ Y.-Z. Zhang, H. O. Jeschke, and R. Valentí, *Phys. Rev. Lett.* **101**, 136406 (2008), arXiv:0809.0145.
 - ⁵ S.-L. Drechsler, O. Volkova, A. N. Vasiliev, N. Tristan, J. Richter, M. Schmitt, H. Rosner, J. Málek, R. Klingeler, A. A. Zvyagin, and B. Büchner, *Phys. Rev. Lett.* **98**, 077202 (2007), arXiv:cond-mat/0701741.
 - ⁶ M. Schmitt, J. Málek, S.-L. Drechsler, and H. Rosner, *Phys. Rev. B* **80**, 205111 (2009)i, arXiv:0911.0307.
 - ⁷ P. W. Anderson, *Mater. Res. Bull.* **8**, 153 (1973).
 - ⁸ J. E. Greedan, *J. Mater. Chem.* **11**, 37 (2001).
 - ⁹ R. Moessner and A. P. Ramirez, *Physics Today* **59(2)**, 24 (2006).
 - ¹⁰ V. Vedral, *Nature* **453**, 1004 (2008).
 - ¹¹ M. P. Shores, E. A. Nytko, B. M. Bartlett, and D. G. Nocera, *J. Am. Chem. Soc.* **127**, 13462 (2005).
 - ¹² J. S. Helton, K. Matan, M. P. Shores, E. A. Nytko, B. M. Bartlett, Y. Yoshida, Y. Takano, A. Suslov, Y. Qiu, J.-H. Chung, D. G. Nocera, and Y. S. Lee, *Phys. Rev. Lett.* **98**, 107204 (2007), arXiv:cond-mat/0610539.
 - ¹³ A. Zorko, S. Nellutla, J. van Tol, L. C. Brunel, F. Bert, F. Duc, J.-C. Trombe, M. A. de Vries, A. Harrison, and P. Mendels, *Phys. Rev. Lett.* **101**, 026405 (2008), arXiv:0804.3107.
 - ¹⁴ R. H. Colman, C. Ritter, and A. S. Wills, *Chem. Mater.* **20**, 6897 (2008), arXiv:0811.4048.
 - ¹⁵ O. Janson, J. Richter, and H. Rosner, *Phys. Rev. Lett.* **101**, 106403 (2008), arXiv:0806.1592.
 - ¹⁶ A. A. Tsirlin and H. Rosner, *Phys. Rev. B* **79**, 214417 (2009), arXiv:0901.4498.
 - ¹⁷ Z. Hiroi, M. Hanawa, N. Kobayashi, M. Nohara, H. Takagi, Y. Kato, and M. Takigawa, *J. Phys. Soc. Jpn.* **70**, 3377 (2001), arXiv:cond-mat/0111127.
 - ¹⁸ D. Kasinathan, K. Koepnik, and H. Rosner, *Phys. Rev. Lett.* **100**, 237202 (2008), arXiv:0805.4080.
 - ¹⁹ M. Yoshida, M. Takigawa, H. Yoshida, Y. Okamoto, and Z. Hiroi, *Phys. Rev. Lett.* **103**, 077207 (2009), arXiv:0906.2846.
 - ²⁰ F. Bert, D. Bono, P. Mendels, F. Ladieu, F. Duc, J.-C. Trombe, and P. Millet, *Phys. Rev. Lett.* **95**, 087203 (2005), arXiv:cond-mat/0507250.
 - ²¹ S. Okubo, H. Ohta, K. Hazuki, T. Sakurai, N. Kobayashi, and Z. Hiroi, *Physica B* **294-295**, 75 (2001).
 - ²² F. Bert, D. Bono, P. Mendels, J.-C. Trombe, P. Millet, A. Amato, C. Baines, and A. Hillier, *J. Phys.: Condens. Matter* **16**, S829 (2004).
 - ²³ H. Yoshida, Y. Okamoto, T. Tayama, T. Sakakibara, M. Tokunaga, A. Matsuo, Y. Narumi, K. Kindo, M. Yoshida, M. Takigawa, and Z. Hiroi, *J. Phys. Soc. Jpn.* **78**, 043704 (2009), arXiv:0902.3028.
 - ²⁴ Z. Hiroi, private communication.
 - ²⁵ P. Sindzingre, arXiv:0707.4264 (unpublished).
 - ²⁶ A. A. Tsirlin and H. Rosner, *Phys. Rev. B* **81**, 024424 (2010), arXiv:0910.2056.
 - ²⁷ O. Janson, A. A. Tsirlin, M. Schmitt, and H. Rosner, *Phys. Rev. B* **82**, 014424 (2010), arXiv:1004.3765.
 - ²⁸ Anisotropic structures require the use of a full-potential code, see H. Rosner, M. Schmitt, D. Kasinathan, A. Ormeci, J. Richter, S.-L. Drechsler, and M. D. Johannes, *Phys. Rev. B* **79**, 127101 (2009).
 - ²⁹ K. Koepnik and H. Eschrig, *Phys. Rev. B* **59**, 1743 (1999).
 - ³⁰ J. P. Perdew and Y. Wang, *Phys. Rev. B* **45**, 13244 (1992).
 - ³¹ See supplementary material for finite lattices used for exact diagonalization, comparison of different exchange-correlation potentials, WF fits, numerical values of transfer integrals, and the basis set used in the DFT calculations.
 - ³² O. Janson, W. Schnelle, M. Schmidt, Y. Prots, S.-L. Drechsler, S. K. Filatov, and H. Rosner, *New J. Phys.* **11**, 113034 (2009), arXiv:0907.4874.
 - ³³ H. Eschrig and K. Koepnik, *Phys. Rev. B* **80**, 104503 (2009)i, arXiv:0905.4844.
 - ³⁴ Only spin degrees of freedom are varied, keeping the orbital GS preserved.
 - ³⁵ The situation is even more complicated because the choice of U_d depends on the relevant orbital¹⁸ and thus different values of U_d should be used for Cu(1) and Cu(2).
 - ³⁶ M. T. Czyżyk and G. A. Sawatzky, *Phys. Rev. B* **49**, 14211 (1994).
 - ³⁷ According to extensive studies of related Cu²⁺ materials, $U_d=10\pm 1.5$ eV for Cu(1) and $U_d=7\pm 1.5$ eV for Cu(2) were chosen as typical values with sizable error bars for the resulting exchange integrals to account for the uncertainties in U_d . An extensive study of the details including the DCC will be published elsewhere.
 - ³⁸ A. Honecker, J. Schulenburg, and J. Richter, *J. Phys.: Condens. Matter* **16**, S749 (2004), arXiv:cond-mat/0309425.
 - ³⁹ J. Richter and J. Schulenburg, *Eur. Phys. J. B* **73**, 117 (2010)i, arXiv:0909.3723.
 - ⁴⁰ Note that due to boundary effects also for the classical model on that finite lattice the expression given above is modified to $J_2^{class} = 0.340|J_1| + 0.166J_{ic}$.
 - ⁴¹ O. A. Starykh, R. R. P. Singh, and G. C. Levine, *Phys. Rev. Lett.* **88**, 167203 (2002), arXiv:cond-mat/0106260.
 - ⁴² R. Coldea, D. A. Tennant, A. M. Tsvelik, and Z. Tylczynski, *Phys. Rev. Lett.* **86**, 1335 (2001), arXiv:cond-mat/0007172.
 - ⁴³ D. C. Cabra, M. D. Grynberg, P. C. W. Holdsworth, A. Honecker, P. Pujol, J. Richter, D. Schmalfuß, and J. Schulenburg, *Phys. Rev. B* **71**, 144420 (2005), arXiv:cond-mat/0404279.
 - ⁴⁴ At low temperatures, finite size effects are strong as evidenced by a sizable deviation between the results for different lattices as well as between $N = 18$ and $N = 24$ curves for the lattice 2.

Supplementary material

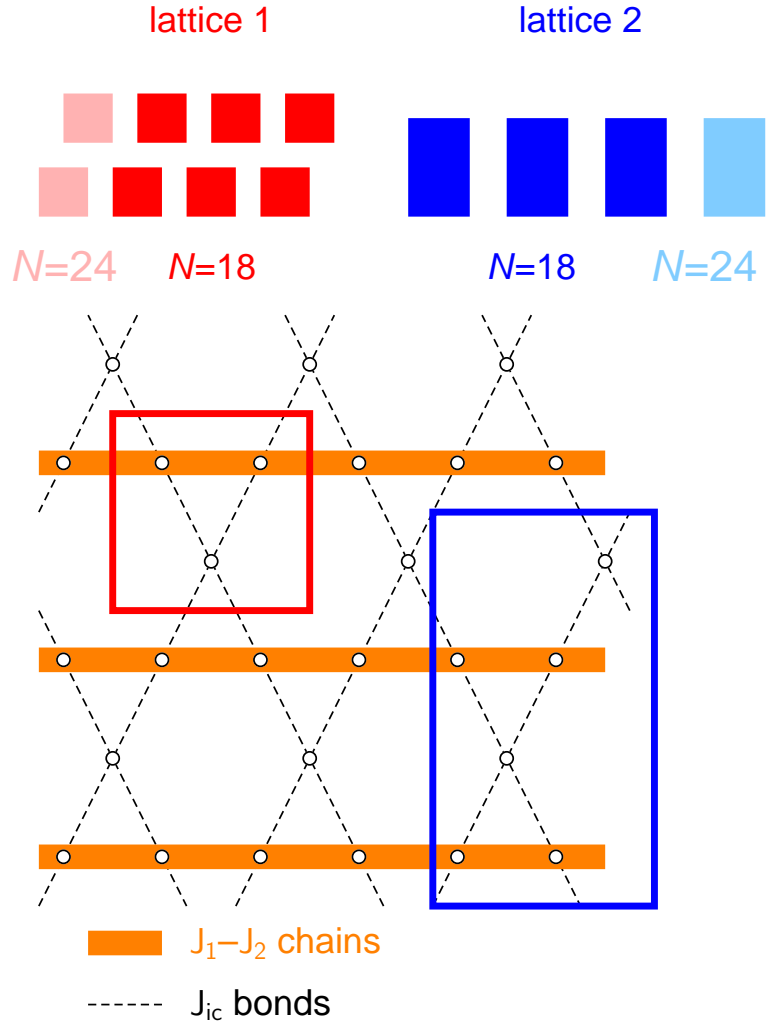
FIG. S1: Finite lattices used for exact diagonalization on $N = 18$ and $N = 24$ sites.

TABLE S1: Basis set used in fpl08.65-32.

atom	core	valence	states	second valence	polarization
Cu	$1s\ 2s\ 2p$	$3s\ 3p\ 4s\ 3d$		$5s\ 4d$	$4p$
V	$1s\ 2s\ 2p$	$3s\ 3p\ 4s\ 3d$		$5s\ 4d$	$4p$
O	$1s$	$2s\ 2p$		$3s\ 3p$	$3d$
H		$1s$		$2s$	$2p$

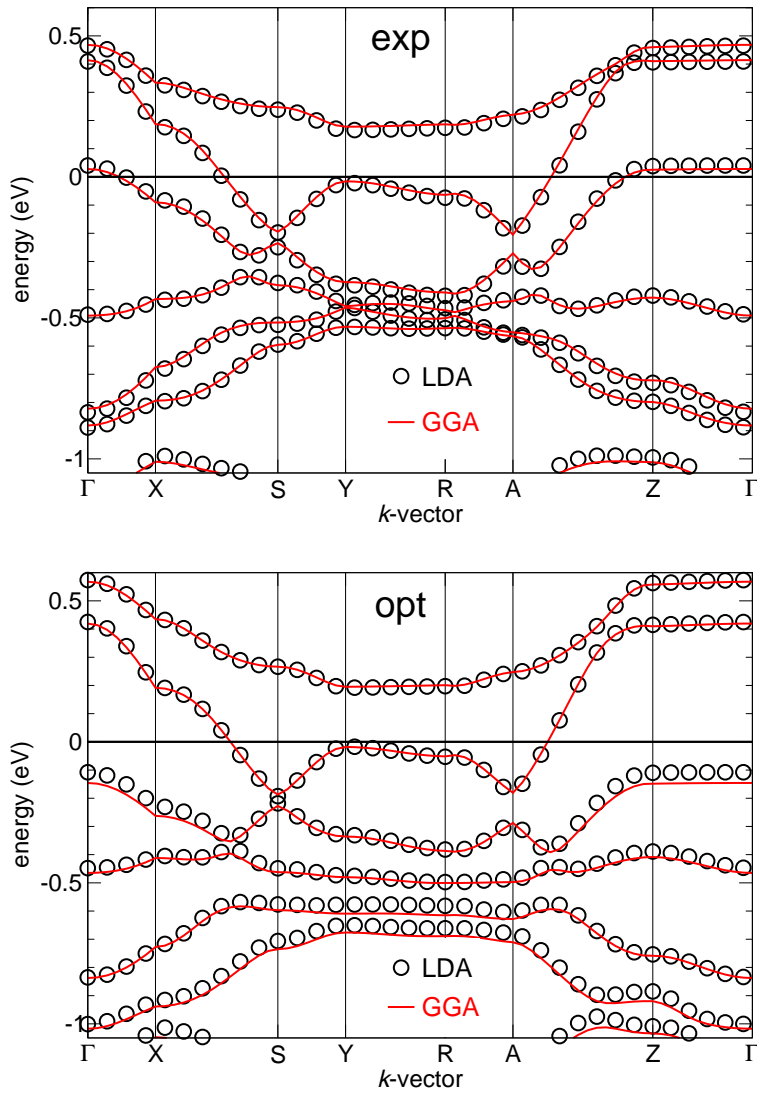


FIG. S2: Comparison of the band structures calculated within the local density approximation (LDA) and the general gradient approximation (GGA) for the experimental (“exp”, top panel) and optimized (“opt”, bottom panel) structures.

TABLE S2: Cells used for LDA and GGA (DFT) as well as spin-polarized LSDA+ U and GGA+ U (DFT+ U) calculations. For each cell, the total number (tot.) as well as the number of symmetrically inequivalent (ineq.) Cu atoms are provided. Basis vectors are given in terms of the unit cell vectors \vec{a} , \vec{b} and \vec{c} . PUC — primitive unit cell, SC — supercell.

cell	Sp. gr.	functional	Cu atoms		basis vectors			k -mesh
			tot.	ineq.				
PUC	$P2/m$	DFT	3	2	$0.5(\vec{a} + \vec{b})$	$0.5(\vec{a} - \vec{b})$	\vec{c}	$12 \times 12 \times 12$
SC1	$P\bar{1}$	DFT	3	3	$0.5(\vec{a} + \vec{b})$	$0.5(\vec{a} - \vec{b})$	\vec{c}	$8 \times 8 \times 8$
		DFT+ U						$4 \times 4 \times 4$
SC2	$P\bar{1}$	DFT	6	6	$0.5(\vec{a} + \vec{b})$	$(\vec{a} - \vec{b})$	\vec{c}	$6 \times 3 \times 6$
		DFT+ U						$3 \times 2 \times 3$
SC3	$P\bar{1}$	DFT	6	6	\vec{a}	\vec{b}	\vec{c}	$4 \times 7 \times 5$
		DFT+ U						$2 \times 4 \times 3$

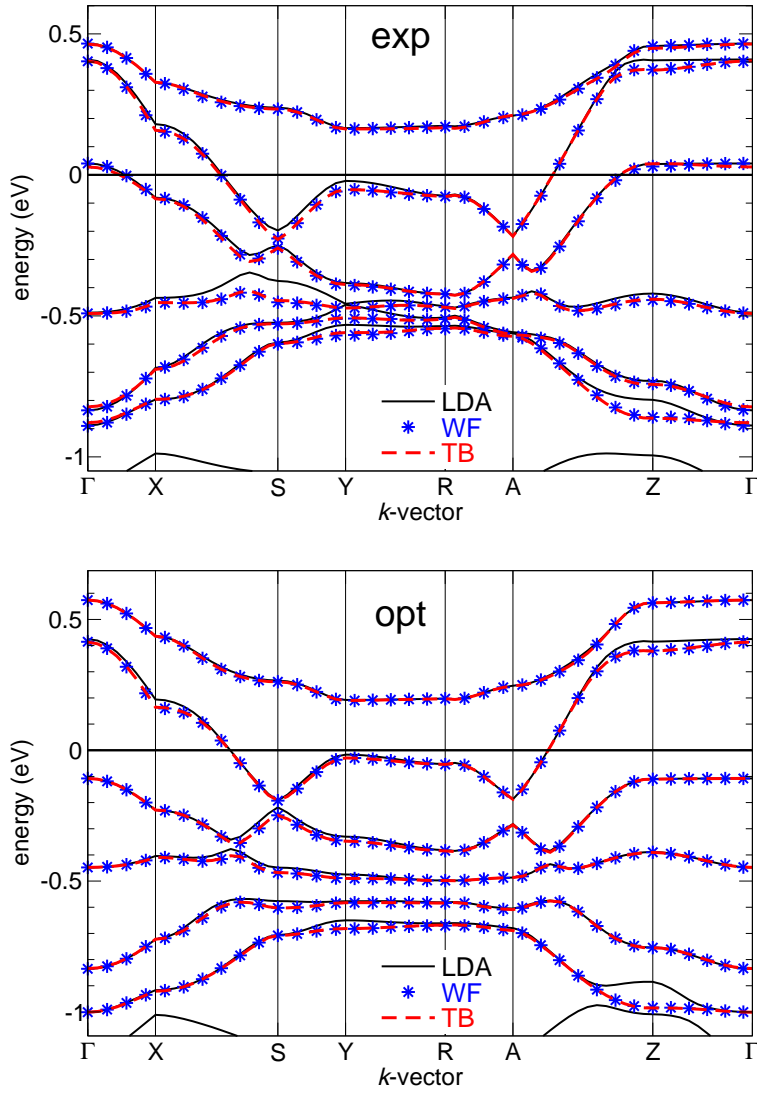


FIG. S3: The Wannier functions fit (WF) and the tight-binding fit (TB) together with the LDA band structure for the experimental (“exp”, top panel) and optimized (“opt”, bottom panel) structures.

TABLE S3: Transfer integrals t as a function of the structural model (exp or opt) and the exchange-correlation potential (LDA or GGA), calculated using the Wannier functions technique. The numbers given correspond to hoppings between the magnetically active orbitals (Cu1 $3d_{3z^2-r^2}$ and Cu2 $3d_{x^2-y^2}$).

	exp		opt	
	LDA	GGA	LDA	GGA
t_1 , meV	91	93	117	119
t_2 , meV	59	57	64	62
t_{ic} , meV	156	156	155	157